



Universiteit
Leiden
The Netherlands

**A refined model of chlorosomal antennae of the Green Bacterium
Chlorobium tepidum from proton chemical shift constrains obtained
with high field 2-D and 3-D MAS NMR dipolar correlation spectroscopy**

Rossum, B.J. van; Steensgaard, D.; Mulder, F.M.; Boender, G.J.; Schaffner, K.; Holzwarth, A.R.; Groot, H.J.M. de

Citation

Rossum, B. J. van, Steensgaard, D., Mulder, F. M., Boender, G. J., Schaffner, K., Holzwarth, A. R., & Groot, H. J. M. de. (2001). A refined model of chlorosomal antennae of the Green Bacterium *Chlorobium tepidum* from proton chemical shift constrains obtained with high field 2-D and 3-D MAS NMR dipolar correlation spectroscopy. *Biochemistry*, 40(6), 1587-1595.
doi:10.1021/bi0017529

Version: Publisher's Version

License: [Licensed under Article 25fa Copyright Act/Law \(Amendment Taverne\)](#)

Downloaded from: <https://hdl.handle.net/1887/3464743>

Note: To cite this publication please use the final published version (if applicable).

A Refined Model of the Chlorosomal Antennae of the Green Bacterium *Chlorobium tepidum* from Proton Chemical Shift Constraints Obtained with High-Field 2-D and 3-D MAS NMR Dipolar Correlation Spectroscopy[†]

B.-J. van Rossum,^{‡,§} D. B. Steensgaard,^{||} F. M. Mulder,^{‡,⊥} G. J. Boender,^{‡,#} K. Schaffner,^{||} A. R. Holzwarth,^{||} and H. J. M. de Groot^{*,‡}

Leiden Institute of Chemistry, Gorlaeus Laboratories, P.O. Box 9502, 2300 RA Leiden, The Netherlands, and Max-Planck-Institut für Strahlenchemie, Postfach 10 13 65 D-45413 Mülheim an der Ruhr, Germany

Received July 27, 2000

ABSTRACT: Heteronuclear 2-D and 3-D magic-angle spinning NMR dipolar correlation spectroscopy was applied to determine solid-state ¹H shifts for aggregated bacteriochlorophyll *c* (BChl *c*) in uniformly ¹³C-enriched light harvesting chlorosomes of the green photosynthetic bacterium *Chlorobium tepidum*. A complete assignment of 29 different observable resonances of the 61 protons of the aggregated BChl *c* in the intact chlorosomes is obtained. Aggregation shifts relative to monomeric BChl *c* in solution are detected for protons attached to rings I, II, and III/V and to their side chains. The 2¹-H₃, 3²-H₃, and 3¹-H resonances are shifted upfield by −2.2, −1, and −3.3 ppm, respectively, relative to monomeric BChl *c* in solution. Although the resonances are inhomogeneously broadened and reveal considerable global structural heterogeneity, the 5-CH and the 7-Me responses are doubled, which provides evidence for the existence of at least two relatively well-defined structurally different arrangements. Ab initio quantum chemical modeling studies were performed to refine a model for the self-assembled BChl *c* with two different types of BChl stacks. The BChl in the stacks can adopt either anti- or syn-configuration of the coordinative bond, where anti and syn designate the relative orientation of the Mg–OH bond relative to the direction of the 17–17¹ bond. The analogy between aggregation shifts for BChl *c* in the chlorosome and for self-assembled chlorophyll *a*/H₂O is explored, and a bilayer model for the tubular supra-structure of sheets of BChl *c* is proposed, from a homology modeling approach.

The first step of the conversion of light energy into chemical free energy in the green photosynthetic bacterium *Chlorobium tepidum* is the absorption of light and transfer of excitation energy in the extramembraneous antenna system, the chlorosome (*I*). Chlorosomes are oblong bodies, around 70 nm wide and 170 nm long. They are found attached to the inside of the cytoplasmic membrane and they are filled with 10–30 rod-shaped elements with a diameter of 10 nm visible in electron microscopy (2). The major component of the chlorosomes of *Chlorobium tepidum* is BChl *c*,¹ with farnesol as the predominant esterifying alcohol (Figure 1). Lipids, protein, carotenoids, and quinones are also present (3, 4). BChl *c* is present in a mixture of homologues and stereoisomers. These differ by the size of the substituent at the 8 and 12 position of the chlorine ring, which can be

methyl, ethyl, propyl, or isobutyl. In addition, both 3¹-R and 3¹-S stereoisomers are present. The BChls are organized in large aggregates stabilized by π–π stacking interactions between the rings, coordination of the Mg²⁺ by the 3¹-hydroxyl group of a neighboring BChl, and hydrogen bonding between the 13¹-carbonyl and the 3¹-hydroxyl groups (3, 5, 6). Two principally different structures are formally in agreement with this basic interaction scheme, closed and open BChl dimers. Although the closed dimer has been proposed for the basic unit in the chlorosomal aggregate (7–9), molecular modeling (10) and various spectroscopic studies (6, 10–13) on in vivo and in vitro aggregates have led us to conclude that the chlorosomal aggregates are based on open dimer structures. According to recent model studies, a minor fraction of 18% 3¹-S–BChl is essential for the formation of chlorosome-type aggregates in vitro (14).

Both the spatial organization and the electronic structure of the microcrystalline BChl in the chlorosomes have been investigated with MAS NMR. 2-D CP/MAS ¹³C homo-

[†] This research was financed in part by the Human Frontiers Science Program (HFSP) Project HFSP-ROG 184/199 and Demonstration Project B104-CT97-2101 of the European Commission and was supported by The Netherlands Foundation for Scientific Research (NWO). H.J.M.d.G. is a recipient of a PIONIER Award of the NWO.

* To whom correspondence should be addressed.

[‡] Leiden Institute of Chemistry.

[§] Present address: FMP, Robert-Rössle-str. 10 D-13125, Berlin, Germany.

^{||} Max-Planck-Institut für Strahlenchemie.

[⊥] Present address: IRI, Delft University of Technology, Mekelweg 15, 2629 JB Delft, The Netherlands.

[#] Present address: ID-DLO, P.O. Box 65, 8200 AB Lelystad, The Netherlands.

¹ Abbreviations: BChl *c*, bacteriochlorophyll *c*; Chl *a*, chlorophyll *a*; COSY, correlation spectroscopy; CP, cross polarization; FID, free induction decay; FSLG, frequency-switched Lee-Goldburg; FTIR, Fourier transform infrared; HPLC, high-performance liquid chromatography; MAS, magic-angle spinning; NMR, nuclear magnetic resonance; RAMP, ramped amplitude; RF, radio frequency; RFDR, radio frequency-driven dipolar recoupling; TPPI, time-proportional phase incrementation; TPPM, two-pulse phase modulation; U-¹³C, uniformly ¹³C enriched; WISE, wide line separation; *n*-D, *n*-dimensional.

Table 1: Solution ($\sigma_{\text{liq}}^{\text{H}}$) and Solid State Shifts (σ_i^{H}) of BChl *c*^a

position	$\sigma_{\text{liq}}^{\text{H}}$ (ppm)	σ_i^{H} (ppm)	ϵ (ppm)
5-H (I)	9.56	7.5 ^b	0.3
5-H (II)	9.56	8.4 ^c	0.3
10-H	9.43	10.0	0.3
3 ¹ -H	6.25	3.0	0.5
13 ² -H ₂	5.09	4.5	0.6
18-H	4.52	4	1
17-H	4.08	4	1
12 ¹ -H ₂	3.97	2 ^d	1
20 ¹ -H ₃	3.72	3 ^e	1
8 ¹ -H ₂	3.67	2 ^f	2
2 ¹ -H ₃	3.30	1.1	0.3
7 ¹ -H ₃ (I)	3.19	3.1 ^g	0.3
7 ¹ -H ₃ (II)	3.19	-0.5 ^h	0.3
17 ² -H ₂	2.35/2.42	1.4	0.3
17 ¹ -H ₂	2.00/2.20	1.4	0.3
3 ² -H ₃	2.01	1.0	0.6
12 ² -H ₃	1.79	2 ^d	2
8 ² -H ₃	1.62	2 ^f	2
18 ¹ -H ₃	1.43	2	1
F1-H ₂	4.31	4.5	0.3
F2-H	5.05	5.4	0.3
F3 ¹ -H ₃	1.5	1.2	0.6
F4-H ₂	1.88	1.8	0.3
F5-H ₂	1.88	2.0	0.3
F6-H	4.95	5.0	0.3
F7 ¹ -H ₃	1.5	1.2	0.6
F8-H ₂	1.88	1.8	0.3
F9-H ₂	1.88	2.0	0.3
F10-H	4.95	5.0	0.3
F11 ¹ -H ₃	1.50	1.5	1
F12-H ₃	1.54	1.2	0.6

^a Solution shifts $\sigma_{\text{liq}}^{\text{H}}$ of monomeric [8-Et,12-Et]BChl *c* in CDCl₃ with 5% CD₃OD and solid-state shifts σ_i^{H} for the BChl *c* in the chlorosomes with estimated errors ϵ . The numbering is according to Figure 1. ^{b,c} Proton signals correlated with the 5-C at 101.2 ppm^b (I) and at 95.1 ppm^c (II). ^d Proton signals correlated with the 12¹- and 12²-Et carbons at 18 and 16 ppm, respectively, resolved from 2-D NMR. ^e A possible splitting of the 20¹-H₃ signal was not resolved from the data. ^f Proton signals correlated with the 8¹- and 8²-Et carbons at 19 and 17 ppm, respectively, resolved from 2-D NMR. ^{g,h} Proton signals correlated with the 7¹-C at 10.4 ppm^g (I) and at 6.6 ppm^h (II).

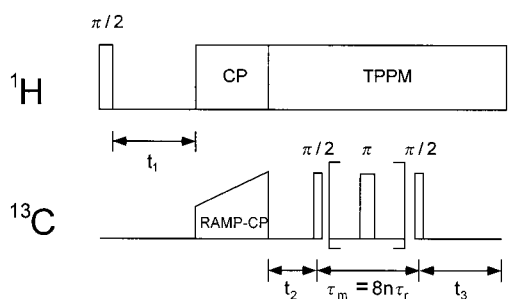


FIGURE 2: NMR pulse sequence used for the 3-D dipolar correlation spectroscopy. Following the cross-polarization (CP) period the protons are decoupled from the carbons with the two-pulse phase modulation (TPPM) technique.

recorded using the CP/WISE technique in the form discussed previously (18, 24). The pulse sequence used for the 3-D (¹H-¹³C-¹³C) spectroscopy is depicted in Figure 2. Following a 90° proton preparation pulse, a time increment t_1 before the cross-polarization allows the observation of the proton evolution with ¹³C detection. Since the efficiency of CP magnetization transfer is very sensitive to RF power instabilities at high MAS frequencies, a RAMP CP sequence (25) was used to broaden the matching profile. The phase of the

¹³C RAMP CP spin-lock pulse was varied according to a TPPI scheme to simulate phase-sensitive detection in t_2 (26), while a TPPI supercycle was applied to the proton preparation pulse to simulate phase-sensitive detection in t_1 . The exchange of polarization through homonuclear ¹³C dipolar interactions during τ_m was promoted by the use of RFDR (27). Short CP contact times of 100 and 250 μ s were used to minimize ¹H homonuclear coherence exchange during CP, while the RFDR mixing time of $\tau_m = 1$ ms was kept short to avoid exchange of proton magnetization via the recoupling of the carbon spins. During the second evolution time t_2 , the mixing period τ_m and the acquisition time t_3 , the protons were decoupled from the carbons by using the TPPM decoupling scheme, which improves the high-field ¹³C resolution considerably (28). The phase-modulation angle and pulse length for the TPPM decoupling were 20° and 8 μ s, respectively. Typical proton and carbon 90° pulse lengths were ~ 4 μ s.

The 2-D heteronuclear (¹H-¹³C) correlation spectrum was recorded with 1024 data points in t_2 and zero filled to 2048 points. A Lorentz-Gauss window with the maximum at 0.1 of the acquisition time and a broadening of 100 Hz was applied prior to Fourier transformation. In the t_1 dimension, 64 points were recorded, which were zero filled to 256 points, and a sine-square apodization, phase-shifted by $\pi/5$, was used. A baseline correction was performed in the t_2 dimension, by applying the linear correction mode from the Aurelia 2.1.1 software package (Bruker, Karlsruhe, Germany) with a baseline-profile file generated with XWIN NMR 1.3 (Bruker, Karlsruhe, Germany). The FIDs of the 3-D (¹H-¹³C-¹³C) dataset were recorded with 512 data points in t_3 and zero filled to 1024 points. In the t_2 dimension 120 points were recorded and zero-filled to 512 points. A Lorentz-Gauss window with the maximum at 0.1 of the acquisition time and a broadening of 100 Hz was applied in both the t_3 and t_2 dimensions prior to Fourier transformation. In the t_1 dimension 56 points were recorded, zero filled to 128 points and processed with a sine-square apodization, phase-shifted by $\pi/3$.

Ab initio quantum chemical calculations were performed using the MacGamess software (29). A small STO-3G basis set was used (30–32).

RESULTS

Since the dipolar interaction between two protons rapidly decreases with their separation, the homonuclear ¹H-¹H interactions for the relatively isolated aromatic protons are much weaker than for protons in the saturated parts of the side chains of the BChl *c* molecule. The joined effect of the effective “dilution” of these protons and an increased proton shift dispersion in a high magnetic field is to attenuate the ¹H homonuclear dipolar line broadening (18). As a result, several of the proton resonances that correlate with ¹³C nuclei in the ring are resolved in the 2-D ¹H-¹³C spectrum of [U-¹³C]-BChl *c* chlorosomes (Figure 3A). For instance, one of the 5 ¹H-¹³C correlation signals and the 10 ¹H-¹³C correlation signal are completely resolved. The proton shifts are 8.4 and 10.0 ppm, respectively, from strong heteronuclear correlations with their respective ¹³C neighbors resonating around 95.1 and 105.6 ppm.

The ¹³C response from the [U-¹³C]BChl *c* in the chlorosomes is inhomogeneously broadened, which has been

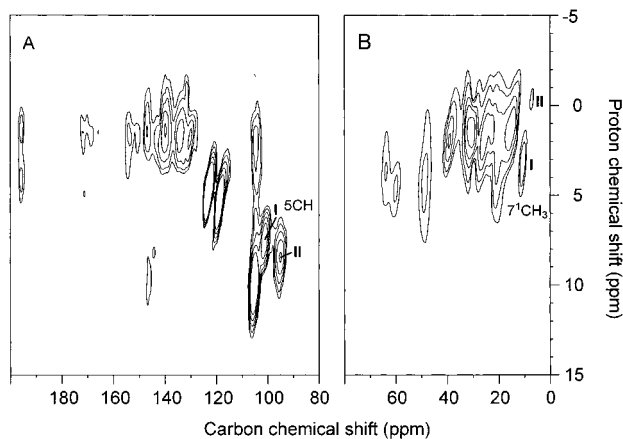


FIGURE 3: Contour plots of the ^{13}C olefinic (A) and ^{13}C aliphatic (B) regions of a 2-D MAS heteronuclear (^1H - ^{13}C) dipolar correlation spectrum of uniformly ^{13}C -enriched chlorosomes collected in a magnetic field of 14.1 T. The spectrum is divided into two parts that are plotted with a different range of contour levels to improve the representation of the data. The correlation spectrum was recorded with a spinning speed $\omega_r/2\pi = 15$ kHz and a CP contact time of 250 μs .

attributed to some structural heterogeneity within the composite BChl *c* aggregate (II). Such disorder will also have an inhomogeneous broadening effect on the proton response, which cannot be relieved with NMR multipulse decoupling techniques. We have briefly explored the effect of FSLG line narrowing in the chlorosomes (33) and have found that the improvement of the resolution is insignificant.²

An effective way to improve the resolution is to add a second ^{13}C dimension. Figure 4 shows a 3-D heteronuclear (^1H - ^{13}C - ^{13}C) dipolar correlation spectrum recorded with the pulse sequence in Figure 2. A single contour level is shown, well above the noise. The resolution in the 3D dataset is sufficient to perform an assignment of proton signals in the aliphatic region. Figure 4, panels B and C, show how the 3-D correlation spectra build up. The ω_2, ω_3 homonuclear carbon slice shown in Figure 4B is the plane associated with a proton shift of ~ 3 ppm in the ω_1 dimension, while the ω_1, ω_3 heteronuclear (^1H - ^{13}C) slice in Figure 4C correlates with a ^{13}C shift near 64 ppm in ω_2 . The line in Figure 4B indicates the correlations of the $3^1\text{-}^{13}\text{C}$ at 63.7 ppm with $3\text{-}^{13}\text{C}$ (139 ppm) and $3^2\text{-}^{13}\text{C}$ (22.2 ppm). Figure 4C shows the same pair of correlations in the proton dimension, which provides the assignment of the $3^1\text{-}^1\text{H}$ response.

The ^1H - ^{13}C - ^{13}C correlations on the diagonal of the carbon-carbon slice in Figure 4B, i.e., the signal with an ω_3 carbon shift of 63.7 ppm in Figure 4C, corresponds with the signal obtained with 2-D CP/WISE (Figure 3). These correlations are superimposed on signals from other components in the sample. For instance, the shoulder with a ^{13}C chemical shift of ~ 60 ppm in Figure 4C originates from a C-OH group of monogalactosyl diacylglyceride in the lipid monolayer that surrounds the chlorosomes (11, 16).

In the 3-D spectrum, we observe a t_2 noise band at a ^{13}C chemical shift of about 30 ppm which is the 3-D analogue

² FSLG decoupling results in a $\sim 50\%$ line-narrowing of the proton resonances of the BChl *c* in the chlorosomes, as compared to the WISE experiments. However, this gain in resolution is almost completely compensated by the scaling of the chemical shift by a factor close to the theoretical value of 0.57 in the Lee-Goldburg experiment.

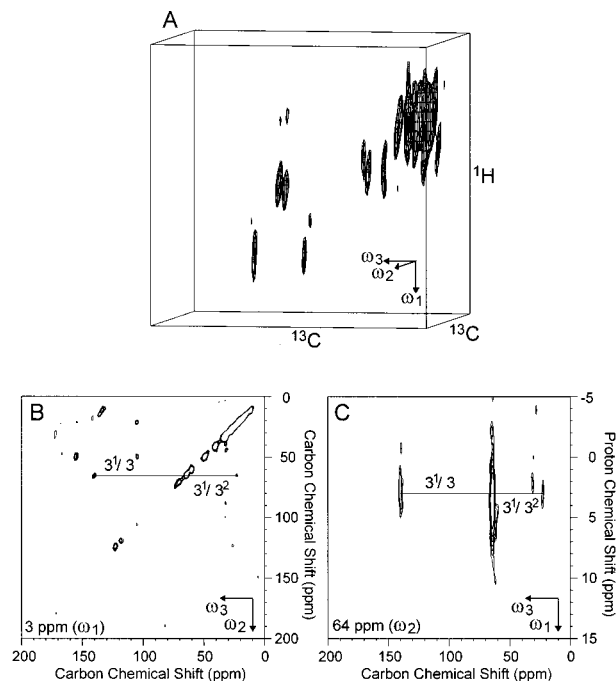


FIGURE 4: Contour plot with a single contour level of a 3-D MAS heteronuclear (^1H - ^{13}C - ^{13}C) dipolar correlation spectrum of uniformly ^{13}C -enriched chlorosomes, recorded with a spinning speed $\omega_r/2\pi = 15$ kHz. The CP time was 100 μs and the polarization transfer time τ_m was 1 ms (A). From the 3-D spectrum, a homonuclear (^{13}C - ^{13}C) slice with a proton shift near 3 ppm (B) and a heteronuclear (^1H - ^{13}C) slice with a carbon shift around 64 ppm (C) were extracted. The extracted slices were plotted with various contour levels.

of t_1 noise in 2-D NMR spectroscopy (34). It runs parallel to the ω_2 axis and is connected to the strongest correlations in the spectrum from the 17^1-CH_2 and 17^2-CH_2 moieties. In the 3-D spectrum, the maximum of the t_2 noise intensity corresponds with a proton chemical shift of about 1.5 ppm, which parallels the assignment of the $17^1\text{-}^1\text{H}_2$ and $17^2\text{-}^1\text{H}_2$ response.

From the 3-D spectrum, all 29 observable proton resonances can be assigned (Table 1). From both the 2-D and the 3-D dipolar correlation spectra, it is found that the 5-CH and 7-Me responses are doubled and give rise to two components in the spectra, designated component I and II. In Figure 3, a fraction of $\sim 57\%$ of $5\text{-}^{13}\text{C}$ (I) resonates with $\sigma_i^{\text{C}} = 101.2$ ppm and correlates with a proton that has $\sigma_i^{\text{H}} = 7.5$ ppm, while the remaining part of $\sim 43\%$ has $\sigma_i^{\text{C}} = 95.1$ ppm for $5\text{-}^{13}\text{C}$ (II) with $\sigma_i^{\text{H}} = 8.4$ ppm for $5\text{-}^1\text{H}$. From Figure 3 it is found that a fraction of $\sim 70\%$ of the 7^1-CH_3 (I) response has $\sigma_i^{\text{C}} = 10.4$ ppm and $\sigma_i^{\text{H}} = 3.1$ ppm. A weaker component II of $\sim 30\%$ is observed with $\sigma_i^{\text{C}} = 6.6$ ppm for the $7^1\text{-}^{13}\text{C}$ and $\sigma_i^{\text{H}} = -0.5$ ppm for the ^1H . The doubling of the ^{13}C resonances is summarized in Table 2. It was recently confirmed by high field homonuclear (^{13}C - ^{13}C) RFDR spectroscopy of the [^{13}C]BChl *c* chlorosomes (35), which revealed additional resolved doublings by ~ 2.3 ppm of the $19\text{-}^{13}\text{C}$ and ~ 1.5 ppm of the $20\text{-}^{13}\text{C}$ responses. The doubling of $19\text{-}^{13}\text{C}$ is confirmed by the 3-D heteronuclear correlation data, while doubling of $20^1\text{-}^1\text{H}_3$ or $18^1\text{-}^1\text{H}_3$ was not resolved from the 3D dataset.

Finally, the $13^1\text{-}^{13}\text{C}$ resonance is visible at 195.8 ppm in Figure 3A, due to magnetization transfer during CP over

Table 2: Carbon Chemical Shifts σ_i^C (ppm) of BChl *c* in Chlorosomes for the Resonances That Are Doubled into Two Components^a

position	σ_{liq}^C (ppm)	σ_i^C (ppm)	
		component I	component II
4-C	145.37	143.5	144.4
5-C	100.03	101.2	95.1
6-C	150.72	149.8	150.5
7-C	133.45	132.3	131.3
7 ¹ -C	10.37	10.4	6.6
8-C	143.39	142.1	140.1
9-C	146.01	146.1	146.8
19-C	167.76	169.0	166.7
20-C	104.74	105.0	103.5

^a The numbering is according to Figure 1. An error of ~ 0.3 ppm is estimated for the solid-state assignment σ_i^C . The σ_{liq}^C (ppm) values are the solution chemical shifts of the monomeric [8-Et,12-Et]BChl *c* in CDCl₃ with 10% CD₃OD (11).

large distances. It has two weak but well-resolved correlations with protons resonating with 1.2 (0.5) and 4.1 (0.5) ppm. In particular, the correlation with proton(s) with $\sigma_i^H = 4.1$ ppm is interesting, since apparently there are no protons in the vicinity of $^{13}\text{C}=\text{O}$ that can possibly account for an intramolecular correlation with $\sigma_i^H = 4.1$ ppm. For instance, the most obvious assignment would be to the nearby $^{13}\text{C}-\text{H}_2$ that resonate around 4.5 ppm. However, the $^{13}\text{C}-\text{H}_2$ give rise to a much broader proton response of ~ 4 kHz due to strong ^1H homonuclear dipolar couplings within the CH₂ moiety. This is difficult to reconcile with the relatively small line width of ~ 2.4 kHz observed in the proton dimension for the correlation with ^{13}C . Other protons near the ^{13}C fail to account for the correlation at 4.1 ppm. These results suggest that it can be associated with intermolecular polarization transfer as discussed below.

DISCUSSION

Effect of Self-Aggregation on the Chemical Shifts. The carbon and proton chemical shifts can be used to extract information at the atomic level about how the electronic structure of the BChl *c* is affected by self-aggregation. Following a similar approach as used previously for the interpretation of the ^{13}C results, aggregation shifts $\Delta\sigma_i^H$ are calculated, which for each site in BChl *c* are defined as $\Delta\sigma_i^H = \sigma_i^H - \sigma_{\text{liq}}^H$. The larger proton aggregation shifts, $|\Delta\sigma_i^H| \geq 1.5$ ppm, are upfield and are detected for 2¹- $^1\text{H}_3$ (−2.2 ppm), 3¹- ^1H (−3.3 ppm), 5- ^1H (I) (−2.1 ppm), 7¹- $^1\text{H}_3$ (II) (−3.7 ppm), and 12¹- $^1\text{H}_2$ (−2 ppm). These aggregation shifts are visualized in Figure 1. Smaller aggregation shifts are observed for 3²- $^1\text{H}_3$ (−1 ppm) and 5- ^1H (II) (−1.2 ppm). In the same figure we have included the carbon aggregation shifts with $|\Delta\sigma_i^C| \geq 1.5$ ppm. The carbon aggregation shifts for 5-, 7-, 7¹-, and 8- ^{13}C , and the proton aggregation shifts for 7¹- $^1\text{H}_3$ of component II are visualized in the right panel in Figure 1.

The proton aggregation shifts of 2¹- $^1\text{H}_3$, 3¹- ^1H , and 12¹- $^1\text{H}_2$ observed for components I and II confirm that for both components the region of the 3-side chain, the 2¹-methyl (ring I), and the region around 12-C and 13-C (rings III/V) are affected similarly by the aggregation processes. This is well in line with the results obtained with ^{13}C correlation

spectroscopy (11, 35). The proton aggregation shifts provide additional support for the parallel chain model, which comprises an arrangement of the BChl *c* in linear stacks by coordination of the oxygen of 3¹-OH to the Mg of the next molecule in the stack (10). In this model, ring I of one molecule is placed over rings III/V of a next BChl *c* in the stack (Figure 5), and substantial ring-current effects are expected for protons that reside above the ring of an adjacent molecule, in line with the pattern of aggregation shifts in Figure 1.

In addition, the upfield aggregation shifts for 2¹- $^1\text{H}_3$, 3¹- ^1H , and 12¹- $^1\text{H}_2$ of both components are in close agreement with the proton aggregation shifts reported from ^1H NMR studies of BChl *c* model aggregates in solution. These oligomers absorb at 740–750 nm, which is in the same range as the BChl *c* in the chlorosomes (36, 37). In this way, the solid-state proton assignments confirm that chlorosome-type BChl *c* aggregates may already be formed in solution (3, 14, 37, 38).

Stacking of BChl c in the Chlorosome. The heteronuclear and homonuclear solid-state NMR results can be used to refine existing models for self-assembled BChl *c* (Figure 5). First, two possible configurations for a 3¹-R-anti (upper panels) and a 3¹-S-syn (lower panels) BChl *c* molecule with Mg coordinated with a methanol were optimized in an ab initio calculation using a small STO-3G basis set. After a full-energy minimization, the Mg was located ~ 0.20 Å above or below the plane formed by the four nitrogen atoms, labeled as syn and anti. The steric hindrance between 2-Me and 20-Me induces a nonplanarity of the macro-aromatic cycle in the region of ring I. The lowest enthalpy in the calculations is obtained when the distortions due to the steric hindrance between the two methyl groups and the metal out of plane distortion are synergetic, leading to a strong out-of-plane deformation in the region of ring I.

In a next step, two bent syn or two bent anti configurations can be placed together in a docking operation to build an optimal dimer structure constrained by the NMR shift and distance information (11, 15, 16, 35). For both syn and anti BChl *c*, a dimer could be formed without any difficulty by coordination of the oxygen of the 3¹-OH to the Mg of the second molecule, with the BChl *c* molecules nearly parallel. This leads to a structure with a distance between the planes of ~ 4.5 Å. This is somewhat more open than in the model of Holzwarth and Schaffner (10) that was based on a BChl *d* analogue, without the 20-Me. There is no evidence for aggregation shifts involving the 20-Me region, which suggests that the conformational differences between the monomer in solution and the BChl *c* in the aggregate are minimal. In a third step, a trimer was built either from three syn or from three anti molecules, with the relative position of the rings approximately the same as in the docked dimer, and with the relative orientation of the rings taken parallel (Figure 5).

Using either syn or anti stacks, it is possible to form layers of parallel stacks, stabilized by the formation of interstack hydrogen bonds between the 3¹-OH groups in one stack to the 13¹=O in a neighboring stack (10). This is a similar arrangement as for ethyl-chlorophyllide *a* (39). Here additional interaction between the stacks is provided by the 17³=O via hydrogen bonding to one of the two water molecules in a hydrogen-bridging network. For BChl *c*,

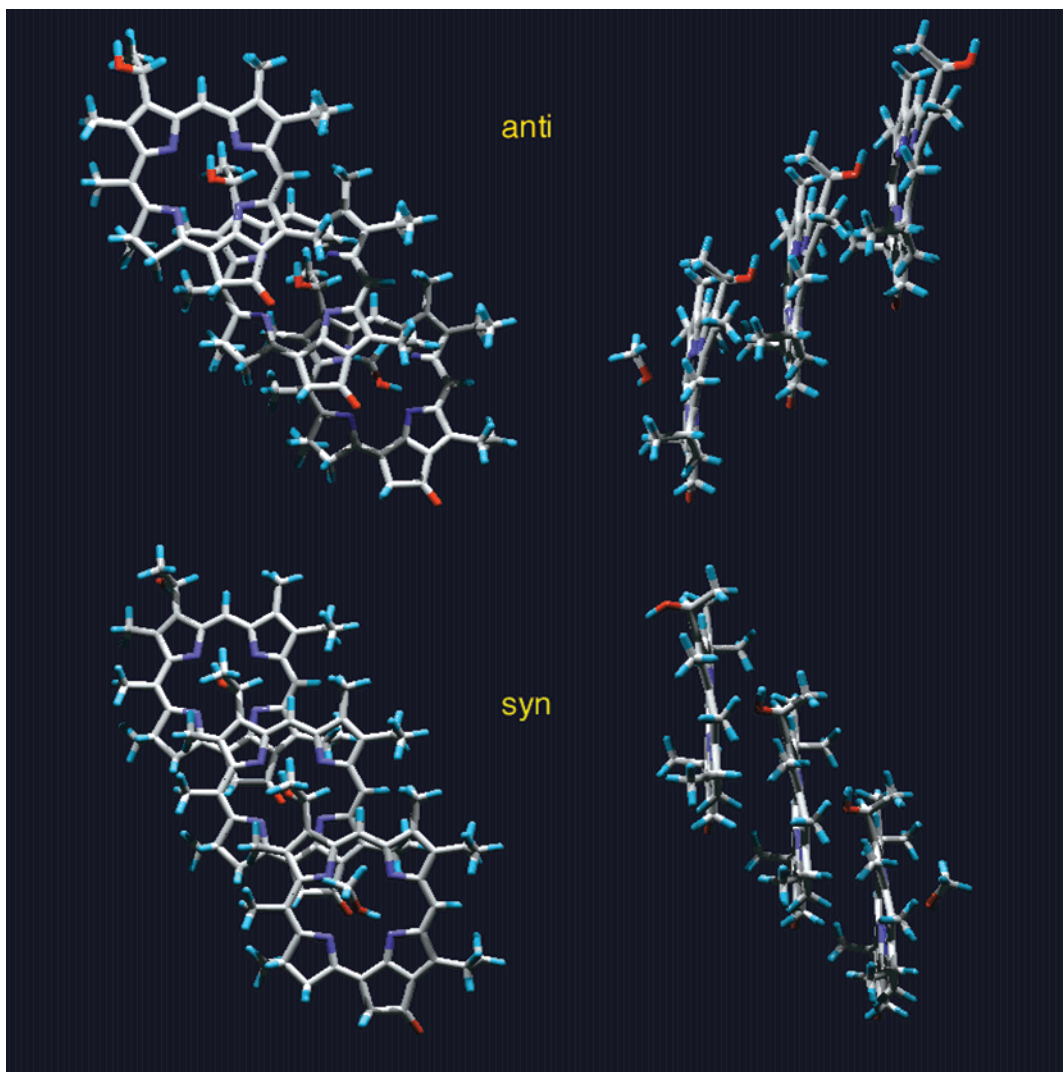


FIGURE 5: Arrangement of BChl *c* rings in 3^1 -R-anti (upper panels) and 3^1 -S-syn stacks (lower panels). The anti and syn configurations would correspond to components **I** and **II**, respectively. The views are chosen to give a clear impression of the structural overlap, which is essential for the correct interpretation of the chemical shift constraints in terms of ring current shifts. In addition, a fragment of a fourth molecule in the stack is included to illustrate the coordination of the Mg.

however, there is no experimental evidence that the $17^3=\text{O}$ is also involved in an interaction. First, FTIR measurements provided evidence for a hydrogen-bonding interaction of the $13^1=\text{O}$ to the 3^1-OH of a second BChl *c*, while no indication was found for an interaction at the $17^3=\text{O}$ (see, e.g., ref 10). Second, complementary evidence is provided by the fact that no water is required for the aggregation of BChl *c*, in contrast with ethyl-chlorophyllide *a*. In absence of water, it is impossible to invoke additional hydrogen-bonding interactions that involve the $17^3\text{-C}=\text{O}$.

If the bent ring structure is predominant in the chlorosome, the shortest intermolecular distances will be between the ring I region of one BChl *c* and the ring IV region of an adjacent molecule. In the linear stack and the 2-D layered sheets, there is little ring overlap between ring III/V region of BChl *c* molecules in different stacks that can lead to additional ring current shifts. This is in line with the pattern of aggregation shifts in Figure 1. It contrasts with the structure of self-assembled Chl *a*/H₂O, where 2-D layered sheets are formed with extended overlap, which gives rise to large ring current shifts of -5 ppm for the NMR resonances of 2^1-H_3 and 12^1-H_3 of the Chl *a* molecule (35, 40).

The anti BChl *c* stack shown in the upper panels of Figure 5 corresponds to the model proposed by Holzwarth and Schaffner (10). The syn trimer in the lower panels of Figure 5 has an opposite sliding direction. This is consistent with the solution NMR work of Mizoguchi et al. (41), in which two different parallel chain stacks with syn and anti configuration were detected. In terms of overlap between the BChl *c* rings, the two structures are virtually mirror images, which can explain why there is no doubling of signals in the overlap region.

The correlation of $13^1\text{-}^{13}\text{C}=\text{O}$ with proton(s) resonating around 4.1 ppm probably involves intermolecular magnetization transfer from the hydrogen-bonded 3^1-OH . Hydrogen-bonded protons can transfer polarization in ~ 250 μs over extended distances, i.e., >2.5 Å (18). Hydroxyl protons resonate in the range 6–10 ppm (42), and a $3^1\text{-O}^1\text{H}$ signal at 4.1 ppm implies a significant upfield shift of $\sim 2\text{--}5$ ppm. In the stacks in Figure 5, the 3^1-OH is located close to the Mg above the macro-aromatic cycle of an adjacent BChl *c* molecule. For such an arrangement, pronounced upfield shifts of up to 5 ppm can be expected due to the BChl *c* ring currents (43). Finally, the correlation of $13^1\text{-}^{13}\text{C}=\text{O}$ with

protons resonating around 1.2 ppm may involve transfer from $3^2\text{-}^1\text{H}_3$. These protons resonate around 1.0 ppm, and can be in close proximity to the $13^1\text{-}^{13}\text{C}$.

The doubling of resonances in the region around rings II and IV shows that there are two structurally different arrangements of aggregated BChl *c*. The difference between the components I and II is most pronounced for ring II, in particular the 7-Me side chain, which points to pronounced ring current effects due to extended overlap between stacks. However, for a layer stabilized by hydrogen bonds the 7-Me is not located above the ring of an adjacent BChl. It is thus difficult to reconcile the NMR data with a monolayer tube stabilized by hydrogen-bonding interactions with the ring V keto group. A doubling of the 5-CH and 7-Me NMR responses is also observed for aggregates prepared from the natural mixture of BChl *c* homologues or from a single pure [8-Et,12-Et]BChl *c* diastereomer (11). This indicates that the formation of two structurally different BChl *c* arrangements in the chlorosomes is not simply due to the presence of different BChl *c* homologues in the chlorosome.

The evidence provided by the solid-state NMR data for the existence of two types of chlorosomal BChl *c* in separate structural arrangements is corroborated by other experimental data. Strong spectral inhomogeneity was observed in chlorosomes of *Prosthecochloris aestuarii* and *Chlorobium phaeovibrioides* that was attributed to different spectral properties of oligomers (44, 45). By deconvolution of linear dichroism and circular dichroism spectra, Matsuura et al. (46) demonstrated the presence of two major spectral components of aggregated BChl *c* in chlorosomes of *Chloroflexus aurantiacus*. A schematic model was proposed in which the two forms of BChl *c* coexist in the rods with the direction of the transition dipole moments nearly parallel to the long axis of the cylinders (47, 48). Somsen et al. (49) confirmed that the variability of the circular dichroism of chlorosomes reflects the presence of at least two structurally different BChl *c* species. Finally, Steensgaard et al. (50) provided evidence for two spectrally different types of BChl *c* within chlorosomes from *Chlorobium tepidum* by monitoring the spectral changes during treatment in acidic buffer. The existence of two spectral forms of BChl *c* absorbing at ~ 740 and ~ 760 nm was demonstrated, with the short wavelength form being more susceptible to reaction with protons.

Refined Model for the Structure of the Aggregated BChl c in the Chlorosomes. The doubling of signals around ring II suggests that some extended intermolecular overlap between layers should be considered an intrinsic property of the self-organization mechanism driving the chlorophyll aggregation process. A schematic model for the BChl *c* aggregates in the chlorosomes can be constructed by exploring the homology with another aggregate, Chl *a*/H₂O. Recently, we have studied the arrangement of [^{13}C] Chl *a*/H₂O with ^{13}C homonuclear and $^1\text{H}\text{-}^{13}\text{C}$ heteronuclear dipolar correlation spectroscopy (40). It was found that Chl *a* forms linear arrays that line up in 2-D layered sheets of aggregated stacks. A similar doubling of the NMR signals as for the BChl *c*, in the 7-Me region, was reported for the Chl *a*/H₂O aggregates. The two structurally different well-defined arrangements of Chl *a* in the sheets can be accommodated by the formation of a bilayer. Such bilayers can form a 3-D laminar structure by interpenetration of the Chl *a* phytol chains or they can form a tubular arrangement. The

formation of a bilayer is energetically favorable, if the electric dipole moments of the two sheets are arranged in an antiparallel way.

Electron microscopy revealed rod-shaped structures with a diameter of ~ 10 nm in the chlorosomes, with a central hole of about ~ 3 nm in diameter (2, 51). There are several ways to form tubular arrangements with sheets of BChl *c*. In the model for the tube proposed previously by Holzwarth and Schaffner (10), the cylinder is formed by a monolayer sheet of aggregated anti BChl *c* that is curved with the farnesyl chains pointing outward. However, this arrangement leaves a large amount of space inside the tubes that has to be filled. This is difficult to reconcile with the MAS NMR data, which show that the major component of the chlorosomes is BChl *c*. In addition, a monolayer tube contrasts with the relatively small hole observed by Cruden and Stanier (51). Alternatively, in analogy with Chl *a*, the cylinder wall can be a bilayer in which the esterifying alcohols of the outer and inner layers are pointing toward the outside and the center of the rod. In this case, the farnesyl chains extending from the inner sheet can fill up the space inside the tube almost completely, leaving a small hole, in agreement with electron microscopy and MAS NMR results. The farnesyl chains of the BChl *c* in the outer tube can extend and interdigitate with the farnesyl chains from the BChl *c* in adjacent tubes or they can be placed against the external wall.

The anti and syn tubes can be combined to form a bilayer tube. In such a model, the number of molecules in the inner layer ought to be smaller than in the outer layer. From 1-D ^{13}C CP/MAS NMR spectra of chlorosome preparations, different signal intensities were found for the $7^1\text{-}^{13}\text{C}$ (I) response relative to the signal from $7^1\text{-}^{13}\text{C}$ (II), in a ratio of about 6:4 between the two components. This may indicate that the upfield shifted 7-Me (II) resonances are associated with a minor syn fraction of BChl *c* in the inner tube. The 7-Me groups are protruding from the sheets and will be positioned at the interface between the two concentric tubes. While the 7-Me groups in the anti sheet point away from the syn sheet, the syn stacks rotate in such a way that the 7-Me region of the molecule is directed toward the anti sheet. The 7-Me groups are therefore in different chemical environments in the contact region between the two layers (cf. Figure 6). This can be expected to contribute to different shifts for the two types of 7-Me groups, due to the combination of ring-current effects, conformational shifts, and the additional strain resulting from the bilayer formation. In our syn and anti models for the stack, the 3^2-methyl groups induce steric hindrance between adjacent BChl *c* and this may contribute to establishing the opposite curvatures of the inner and outer layer. Alternatively, differences in the stereochemistry of the 3-side chain, which were not taken into account in our modeling attempts thus far, may be essential to invoke bending in opposite directions.

In 1-D ^{13}C CP/MAS NMR spectra, it was observed that the line width of the $7^1\text{-}^{13}\text{C}$ (II) signal is about 350 Hz, while the width of the response from $7^1\text{-}^{13}\text{C}$ (I) is ~ 220 Hz. This suggests additional inhomogeneous broadening of the $7^1\text{-}^{13}\text{C}$ (II) signal. In the $^1\text{H}\text{-}^{13}\text{C}$ dataset in Figure 3, the correlation with $7^1\text{-}^{13}\text{C}$ (II) is tilted and the additional broadening dispersion of the carbon response correlates with the broadening dispersion of the proton response. This is in line with the assignment of the 7-Me (II) resonances to the

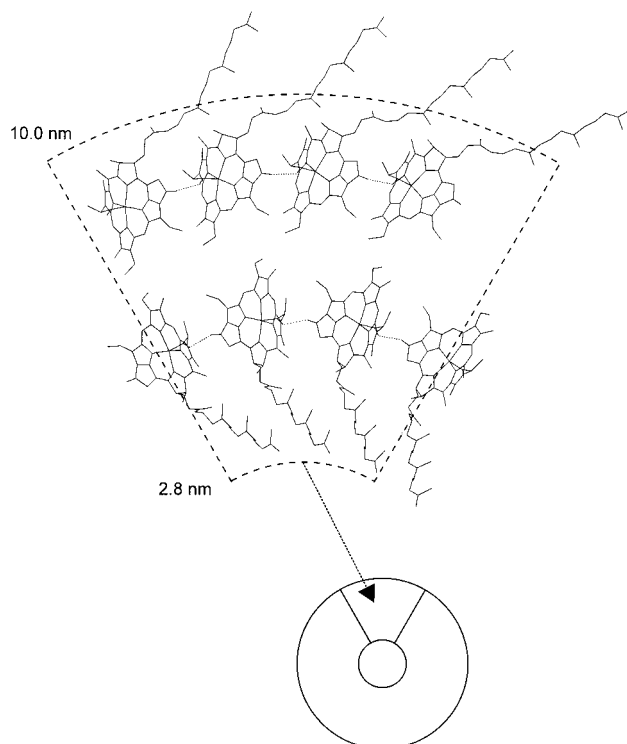


FIGURE 6: Schematic representation of a radial wall section of a bilayer tube formed from curved 2-D sheets of anti (I) and syn stacks (II). The chlorin rings are completed with the farnesyl tails, which were not included in the *ab initio* calculations. The curvature leads in a natural way to the dimensions determined with electron microscopy. The direction of the stacks is perpendicular to the plane of the paper. The dotted lines indicate hydrogen bonds between $^{13}\text{C}=\text{O}$ and $^3\text{C}-\text{OH}$ of adjacent stacks. In reality, the interface between the outer and inner tube is expected to be more dense than in this schematic representation, to account for the aggregation shifts of the 7^1 methyls.

inner tube in the schematic model in Figure 6. The 7-Me groups protruding from the syn sheet are more exposed and subject to inevitable heterogeneity at the interface, considering that BChl *c* in the inner and outer tube will not completely line up and the interface may be distorted in the sample used in the NMR studies.

Finally, comparison of the proton responses of the farnesyl chain of BChl *c* with the resonances of the phytyl chain of Chl *a* reveals a significant excess line broadening of the BChl *c* farnesyl proton signals. For Chl *a*, the phytyl chains of neighboring bilayers form an ordered interdigitating network. The broadened signals of the BChl *c* tails suggest that the farnesyl chains are somewhat disordered and may exhibit a random folding. In addition, we have demonstrated recently that the NMR relaxation parameters of the rigid BChl *c* ring system and the farnesyl chain are highly similar, from which it was concluded that at least a substantial fraction of the farnesyl chains should be relatively immobile (33). This is in line with the model of a bilayer cylinder, where the fatty alcohol chains on the inside will be rigidly held in place.

A bilayer tube composed of an anti outer layer and a syn inner layer of aggregated BChl *c* can thus be reconciled with the solid-state NMR results and the available microscopy data (2, 51, 52). It is tempting to correlate the reported heterogeneity of optical characteristics of the chlorosomal with our findings of structural heterogeneity in the BChl aggregate on the molecular level (44, 50). However, the

earlier reports suggest heterogeneity on a larger scale, which may not directly relate to the detection of two different types of BChl *c* stacks. In addition, the aggregate structure imposes strong excitonic interactions of the BChls both within a single stack and between adjacent rods (53). This means that care should be taken when adapting conclusions from observations of the data from optical spectroscopy to the aggregate structure on a molecular level. Currently exciton calculations are in progress to model the effect of a double layer structure on the optical spectra.

CONCLUSIONS

The arrangement of BChl *c* was studied in uniformly ^{13}C -labeled intact chlorosomes of a green photosynthetic bacterium using high-field 2-D (^1H - ^{13}C) and 3-D (^1H - ^{13}C - ^{13}C) heteronuclear MAS NMR dipolar correlation spectroscopy. From the correlation spectra, it was possible to assign all observable proton resonances. The solid-state ^1H assignment was used to calculate proton aggregation shifts relative to monomeric BChl *c* in solution. The pattern of aggregation shifts corroborates the parallel chain model. A doubling of the 5-CH and the 7-Me NMR resonances was observed, which provides strong evidence for the presence of at least two structurally different well-defined arrangements of the BChl *c* in the chlorosomes. The NMR data for $[\text{U}-^{13}\text{C}]\text{BChl } c$ chlorosomes and *in vitro* $[\text{U}-^{13}\text{C}]\text{BChl } c$ aggregates are remarkably similar to those obtained from aggregates of $[\text{U}-^{13}\text{C}]\text{Chl } a/\text{H}_2\text{O}$. By comparing the NMR results with other available NMR and structural data in a homology study, a bilayer tube is proposed for the arrangement of BChl *c* that is composed of sheets of stacks with opposite sliding direction.

ACKNOWLEDGMENT

We wish to thank C. Erkelens for support during various stages of the work. T. S. Balaban is gratefully acknowledged for his pioneering work in growing and isolating uniformly labeled chlorosome preparations during earlier stages of this project.

REFERENCES

- Olson, J. M. (1998) *Photochem. Photobiol.* 67, 61–75.
- Staelin, L. A., Golecki, J. R., and Drews, G. (1980) *Biochim. Biophys. Acta* 589, 30–45.
- Balaban, T. S., Leitich, J., Holzwarth, A. R., and Schaffner, K. (2000) *J. Phys. Chem.* 104, 1362–1372.
- Blankenship, R. E., Olson, J., and Miller, M. (1995) in *Anoxygenic Photosynthetic Bacteria* (Blankenship, R. E., Madigan, M. T., and Bauer, C. E., Eds.) pp 399–435, Kluwer Academic Publishers, Dordrecht.
- Bystrova, M. I., Mal'gosheva, I. N., and Krasnovskii, A. A. (1979) *Mol. Biol. Engl. Trans.* 13, 440–451.
- Hildebrandt, P., Tamiaki, H., Holzwarth, A. R., and Schaffner, K. (1994) *J. Phys. Chem.* 98, 2192–2197.
- Nozawa, T., Nishimura, M., Hatano, M., Hayashi, H., and Shimada, K. (1985) *Biochemistry* 24, 1890.
- Brune, D. C., King, G. H., and Blankenship, R. E. (1988) in *Photosynthetic Light-Harvesting Systems* (Scheer, H., and Schneider, S., Eds.) pp 141–151, de Gruyter, Berlin.
- Umetsu, M., Wang, Z. Y., Zhang, J., Ishii, T., Uehara, K., Inoko, Y., Kobayashi, M., and Nozawa, T. (1999) *Photosynth. Res.* 60, 229.
- Holzwarth, A. R., and Schaffner, K. (1994) *Photosynth. Res.* 41, 225–233.

11. Balaban, T. S., Holzwarth, A. R., Schaffner, K., Boender, G.-J., and De Groot, H. J. M. (1995) *Biochemistry* 34, 15259–15266.
12. Balaban, T. S., Taniaki, H., Holzwarth, A. R., and Schaffner, K. (1997) *J. Phys. Chem. B* 101, 3424.
13. Chiefari, J., Griebenow, K., Fages, F., Griebenow, N., Balaban, T. S., Holzwarth, A. R., and Schaffner, K. (1995) *J. Phys. Chem.* 99, 1357.
14. Mizoguchi, T., Hara, K., Nagae, H., and Koyama, Y. (2000) *Photochem. Photobiol.* 71, 596–609.
15. Boender, G.-J., Balaban, T. S., Holzwarth, A. R., Schaffner, K., Raap, J., Prytulla, S., Oschkinat, H., and De Groot, H. J. M. (1995) in *Photosynthesis: From Light to Biosphere* (Mathis, P., Ed.) Vol. 1, pp 347–350, Kluwer Academic Publishers, Boston, Dordrecht, London.
16. Boender, G.-J. (1996) Ph.D. Thesis, University of Leiden.
17. Schaffner, K., and Holzwarth, A. (1996) in *Jahrbuch 1996 der Deutschen Akademie der Naturforscher Leopoldina (R.3)* 42, pp 205–220.
18. Van Rossum, B.-J., Boender, G.-J., and De Groot, H. J. M., (1996) *J. Magn. Reson. A* 120, 274–277.
19. Katz, J. J., and Brown, C. E. (1983) *Bull. Magn. Reson.* 5, 3–49.
20. Abraham, R. J., Rowan, A. E., Goff, D. A., Mansfield, K. E., and Smith, K. M. (1989) *J. Chem. Soc. Perkin Trans. II*, 1633–1641.
21. Smith, K. M., Bobe, F. W., Goff, D. A., and Abraham, R. J. (1986) *J. Am. Chem. Soc.* 108, 1111–1120.
22. Abraham, R. J., and Rowan, A. E. (1991) in *Chlorophylls* (Scheer, H., Ed.) pp 797–834, CRC Press, Boca Raton, Florida.
23. De Groot, H. J. M., Copié, V., Smith, S. O., Allen, P. J., Winkel, C., Lugtenburg, J., Herzfeld, J., and Griffin, R. G. (1988) *J. Magn. Reson.* 77, 251–257.
24. Schmidt-Rohr, K., Clauss, J., and Spiess, H. W. (1992) *Macromolecules* 25, 3273–3277.
25. Metz, G., Wu, X., and Smith, S. O. (1994) *J. Magn. Reson. A* 110, 219–227.
26. Marion, D., and Wüthrich, K. (1983) *Biochem. Biophys. Res. Commun.* 113, 967.
27. Bennet, A. E., Ok, J. H., Griffin, R. G., and Vega S. (1992) *J. Chem. Phys.* 96, 8624–8627.
28. Bennet, A. E., Rienstra, C. M., Auger, M., Lakshmi, K. V., and Griffin, R. G. (1995) *J. Chem. Phys.* 103, 6951–6957.
29. Schmidt, M. W., Baldrige, K. K., Boatz, J. A., Elbert, S. T., Gordon, M. S., Jensen, J. J., Koseki, S., Matsunaga, N., Nguyen, K. A., Su, S., Windus, T. L.; Dupuis, M., and Montgomery, J. A. (1993) *J. Comput. Chem.* 14, 1347–1363.
30. Hehre, W. J., Stewart, R. F., and Pople J. A. (1969) *J. Chem. Phys.* 51, 2657–2664.
31. Hehre, W. J., Ditchfield, R., Stewart, R. F., and Pople, J. A. (1970) *J. Chem Phys.* 52, 2769–2773.
32. Gordon, M. S., BJORKE, M. D., Marsh, F. J., and Korth, M. S. (1978) *J. Am. Chem. Soc.* 100, 2670–2678.
33. Van Rossum, B.-J., Van Duyll, B. Y., Steensgaard, D. B., Balaban, T. S., Holzwarth, A. R., Schaffner K., and De Groot, H. J. M. (1998) in *Photosynthesis: Mechanisms and Effects* (Garab, G., Ed.) Vol. I, pp 117–120, Kluwer Academic Publishers, Dordrecht, The Netherlands.
34. Mehlkopf, A. F., Korbee, D., Tiggelman, T. A., and Freeman, R. (1984) *J. Magn. Reson.* 58, 315–323.
35. Van Rossum, B.-J., Boender, G. J., Mulder, F. M., Raap, J., Balaban, T. S., Holzwarth, A. R., Schaffner, K., Prytulla, S., Oschkinat, H., and De Groot, H. J. M. (1998) *Spectrochim. Acta A* 54, 1167–1176.
36. Mizoguchi, T., Limantara, L., Matsuura, K., Shimada, K., and Koyama, Y. (1996) *J. Mol. Struct.* 379, 249–265.
37. Mizoguchi, T., Matsuura, K., Shimada, K., and Koyama, Y. (1996) *Chem. Phys. Lett.* 260, 153–158.
38. Smith, K. M., Kehres, L. A., and Fajer, J. (1983) *J. Am. Chem. Soc.* 105, 1387–1389.
39. Chow, H. C., Serlin, R., and Strouse, C. E. (1975) *J. Am. Chem. Soc.* 97, 7230–7237.
40. van Rossum et al. (2000) Submitted for publication.
41. Mizoguchi, T., Sakamoto, S., Koyama, Y., Ogura, K., and Inagaki, F. (1998) *Photochem. Photobiol.* 67, 239–248.
42. BMRB database, http://www.bmrb.wisc.edu/ref_info/statsel.htm.
43. Giessner-Prettre, C., and Pullman, B. (1971) *J. Theor. Biol.* 31, 287–294.
44. Otte, S. C. M., Van der Heiden, J. C., Pfennig, N., and Amesz, J. (1991) *Photosynth. Res.* 28, 77–87.
45. Van Noort, P. I., Francke, C., Schoumans, N., Otte, S. C. M., Aartsma, T. J., and Amesz, J. (1994) *Photosynth. Res.* 41, 193–203.
46. Matsuura, K., Hirota, M., Shimada, K., and Mimuro, M. (1993) *Photochem. Photobiol.* 57, 92–97.
47. Mimuro, M., Hirota, M., Nishimura, Y., Moriyama, T., Yamazaki, I., Shimada, K., and Matsuura, K. (1994) *Photosynth. Res.* 41, 181–191.
48. Mimuro, M., Nishimura, Y., Yamazaki, I., Kobayashi, M., Wang, Z. Y., Nozawa, T., Shimada, K., and Matsuura, K. (1996) *Photosynth. Res.* 48, 263–270.
49. Somsen, O. J. G., Van Grondelle, R., and Van Amerongen, H. (1996) *Biophys. J.* 71, 1934–1951.
50. Steensgaard, D. B., Matsuura, K., Cox, R. P., and Miller, M. (1997) *Photochem. Photobiol.* 65, 129–134.
51. Cruden, D. L., and Stanier (1970) *Arch. Microbiol.* 72, 115–134.
52. Staehelin, L. A., Golecki, J. R., Fuller, R. C., and Drews, G. (1978) *Arch. Mikrobiol.* 119, 269–277.
53. Prokhorenko, V., I., Steensgaard, D. B., and Holzwarth, A. R. (2000) *Biophys. J.* (in press).

BI0017529